minerals

MDPI

Article

Metamorphic Ages and *PT* Conditions of Amphibolites in the Diebusige and Bayanwulashan Complexes of the Alxa Block, North China Craton

Feng Zhou [1], Longlong Gou [1,*], Xiaofei Xu [1,2] and Zhibo Tian [1]

[1] State Key Laboratory of Continental Dynamics, Department of Geology, Northwest University, Xi'an 710069, China; xuxiaofei@kust.edu.cn (X.X.)
[2] Faculty of Land Resources Engineering, Kunming University of Science and Technology, Kunming 650093, China
* Correspondence: LLgou@nwu.edu.cn

Abstract: The metamorphism and geological significance of amphibolites in the Diebusige and Bayanwulashan Complexes of the eastern Alxa Block, North China Craton, were poorly understood until now. This study presents the results of petrology, laser ablation inductively coupled plasma mass spectrometry (LA-ICP-MS) zircon U–Pb analysis, phase equilibrium modeling and geothermobarometry for these rocks. The peak mineral assemblage of clinopyroxene + hornblende + plagioclase + K-feldspar + ilmenite + quartz + melt is inferred for amphibolite sample ALS2164 in the Diebusige Complex. Correspondingly, the peak mineral assemblage of clinopyroxene + hornblende + plagioclase ± K-feldspar + ilmenite + quartz + melt is identified for amphibolite sample ALS2191 in the Bayanwulshan Complex. Phase equilibrium modelling constrained the peak metamorphic condition of amphibolite sample ALS2164 in the Diebusige Complex to be 825–910 °C/7.2–10.8 kbar, which is similar to that (800–870 °C/7.0–10.7 kbar) of amphibolite sample ALS2191 in the Bayanwulashan Complex. Hbl–pl–qz thermobarometry yielded the metamorphic *PT* conditions of 732–810 °C/3.0–6.7 kbar for these amphibolites, which are consistent with the average temperatures of 763 °C, 768 °C and 780 °C calculated by Ti-zircon thermometry. As a result, phase equilibrium modelling yielded wide *PT* condition ranges of 800–910 °C/7.0–10.8 kbar, the lower limit of which is consistent with the upper limit of estimates by the hbl–pl–qz thermobarometer. In addition, LA-ICP-MS U–Pb analysis on metamorphic zircons yielded weighted mean $^{207}Pb/^{206}Pb$ ages of 1901 ± 22–1817 ± 21 Ma, which represent the timing of amphibolite-facies metamorphism. As a whole, the *PT* estimates display a high geothermal gradient, which is consistent with coeval ultrahigh-temperature metamorphism and associated mantle-derived mafic-ultramafic rocks in the Diebusige Complex. Combing this information with the previously published data from the Diebusige Complex, an extensional setting after continental collision is inferred for the eastern Alxa Block during the late Paleoproterozoic. The HREE enrichment patterns of metamorphic zircons from the amphibolites in this study are in agreement with that these amphibolites formed at relatively shallower crust than the garnet-bearing mafic granulites in the Diebusige Complex.

Keywords: amphibolites; the Alxa Block; the Khondalite Belt; zircon U-Pb age; extensional setting

Citation: Zhou, F.; Gou, L.; Xu, X.; Tian, Z. Metamorphic Ages and *PT* Conditions of Amphibolites in the Diebusige and Bayanwulashan Complexes of the Alxa Block, North China Craton. *Minerals* **2023**, *13*, 1426. https://doi.org/10.3390/min13111426

Academic Editors: Jin Liu, Jiahui Qian, Xiaoguang Liu and Silvana Martin

Received: 29 August 2023
Revised: 31 October 2023
Accepted: 3 November 2023
Published: 9 November 2023

1. Introduction

Amphibolites, one of the common metabasic rocks in metamorphic terranes from Precambrian to Phanerozoic, can provide valuable information for the study of geological processes [1,2]. Previous experimental studies suggest that amphibolites can be stable in a relatively wide *PT* range of 0–15 kbar/500–950 °C [3–7]. Afterwards, some researchers proposed that the upper temperature limit of amphibolite-facies metamorphism is 700–850 °C [8–10], which is lower than the results determined by experimental studies. In

terms of origin, amphibolite can be formed by metamorphism of mafic igneous rock (ortho-amphibolite) or sedimentary tuff (para-amphibolite) (two different origins of amphibolites in the Xiangshan area of Jiangxi province [11]). Amphibolite may be prograde products of Barrow-type metamorphism [4,12,13] with a clockwise *P*–*T* path, reflecting the collision thickening environment, such as the amphibolite in the Wutai–Hengshan area [14]. It can also be retrograde products of overprinted high-pressure/ultrahigh-pressure (HP/UHP) eclogites, where the *P*–*T* path is dominated by decompression [7,15,16], such as the amphibolite in the Qingyouhe area of Qinling Complex [17]. The formation of amphibolite may be related to the underplating of mantle-derived magmas, which is characterized by an anticlockwise *P*–*T* path (amphibolite in the northern Liaoning Complex [18]). In addition, amphibolite with a decompressional heating *P*–*T* segment can reflect an extensional setting that developed on a previous orogen (amphibolite in the Xilingol Complex of Inner Mongolia [19]).

The Alxa Block is located in the westernmost part of the North China Craton (NCC), adjacent to the Khondalite Belt (KB) (Figure 1a). In recent decades, some researchers considered that the Alxa Block has an affinity to the Yangtze Craton or the Tarim Craton due to the identification of the Neoproterozoic magmatism [20,21], whereas others thought that the Alxa Block was the western extension of the Yinshan Block, NCC [22,23]. Additionally, some scholars argued that the Alxa Block is an independent block or a microcontinental block in a Paleozoic orogenic belt [24–26]. Recently, more and more evidence has supported the Alxa Block as the westward extension of the KB due to the discovery of ca. 1.96–1.83 Ga metamorphism, ca. 2.3–2.0 Ga magmatism and small-scale Neoarchean magmatism in this block [27–35]. Therefore, the relationship between the Alxa Block and the NCC has become the focus of controversy, and research on metamorphism can provide important insights for solving this dispute. Furthermore, the Diebusige and Bayanwulashan Complexes distributed discontinuously along the eastern Alxa Block (Figure 1b) are composed of felsic orthogneiss, amphibolite lenses or interlayers, and a few metasedimentary rocks [36,37]. Previous work revealed that these amphibolite lenses or interlayers had metamorphic ages of ca. 1.93–1.81 Ga [36,37], which are comparable to published metamorphic ages of ca. 1.96–1.83 Ga for high- to ultrahigh-temperature (HT–HUT) metamorphic rocks in the Diebusige Complex [33–35]. Due to the lack of detailed metamorphic *PT* condition calculations for these amphibolites, their relationship with HT–UHT metamorphic rocks, and the implications for tectonic evolution of the Alxa Block are unclear until now.

In this study, we describe amphibolites in the Diebusige and Bayanwulashan Complexes of the eastern Alxa Block, NCC. Detailed studies of petrology, U–Pb ages and trace elements of metamorphic zircons, and metamorphic *PT* condition calculations using phase equilibrium modelling and conventional thermobarometries are used to reveal the metamorphic ages and characteristics of these amphibolites. Metamorphic ages and *PT* conditions constrained for amphibolites in this study, coupled with previously published data in the region, provide us new insight to elucidate their tectonic significance of the Alxa Block.

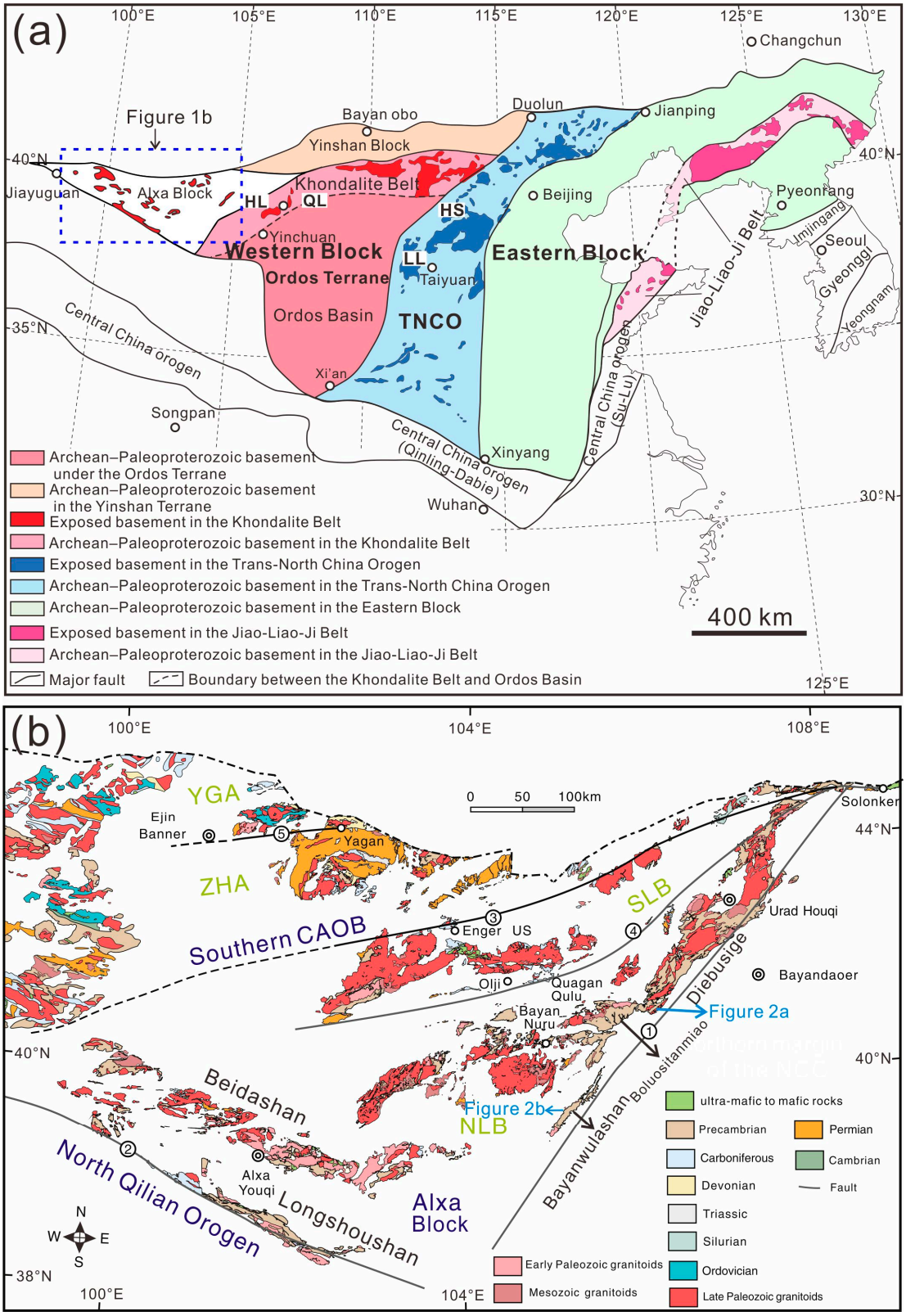

Figure 1. (**a**) Simplified tectonic sketch map of the North China Craton (NCC) showing the location of the Alxa Block and (**b**) geological map of the Alxa Block (revised from BGMRIM (1991) [38]). CAOB, Central Asian Orogenic Belt; YGA, the Yagan arc; ZHA, the Zhusileng–Hangwula arc; SLB, the Shalazhashan belt; NLB, the Nuru–Langshan belt. ① The Langshan fault, ② the Longshoushan fault, ③ the Enger US fault, ④ the Badain Jaran fault, ⑤ the Yagan fault.

2. Geological Setting

The westernmost part of the NCC, termed as the Alxa block, is bounded by the Central Asian Orogenic Belt and the Qilian Orogen to the south, respectively (Figure 1a,b). The Alxa Block is mainly covered by Cenozoic sediments, and the outcrops of Precambrian metamorphic basement rocks are sporadically exposed in the western and eastern parts of the block (Figure 1b). The Precambrian basement of the western Alxa Block is mainly composed of the Longshoushan and Beidashan Complexes [27,30,39,40] (Figure 1b), and the Precambrian basement of the eastern Alxa Block consists of the Diebusige, Bayanwulashan and Boluositanmiao Complexes [29,36,37,41,42] (Figure 1b).

2.1. The Western Alxa Block

The Longshoushan Complex is composed of felsic gneisses, amphibolites and metasedimentary rocks [30,31,43–46]. The crystallization ages for the protolith of felsic gneisses were constrained to be ca. 2.35–2.01 Ga, and their metamorphic ages vary from ca. 1.97 to 1.84 Ga [30,31,43–45,47]. The metamorphic ages of amphibolites have been determined at ca. 1.85 Ga [31]. Metasedimentary rocks have detrital zircon ages ranging from ca. 3.0 to 1.98 Ga, and their metamorphic ages are ca. 1.96–1.92 Ga [31,45,46].

The Beidashan Complex is predominantly composed of granodioritic–trondhjemitic gneisses, whose protolith crystallization ages are ca. 2.84–2.50 Ga, and their metamorphic ages are constrained at ca. 2.53–2.47 Ga and ca. 1.87–1.83 Ga [27,39]. The sequence of metamorphic events is similar to those of the NCC, thereby the Alxa Block was considered as the western extension of the Khondalite Belt or an integrated component of the NCC [27,45].

2.2. The Eastern Alxa Block

The Diebusige Complex mainly consists of felsic gneisses, amphibolite, and minor metasedimentary rocks (e.g., banded iron formations and pelitic gneisses) [29,32–36,42]. SHRIMP and SIMS zircon U–Pb dating yielded protolith crystallization ages of ca. 1.98–1.97 Ga and the metamorphic ages of ca. 1.93 and 1.80 Ga for felsic gneisses [29,36,42]. The metamorphic ages of 1.84 and 1.85 Ga were obtained for magnetite quartzites, and peak metamorphic temperature was estimated at ~860–800 °C by the two-pyroxene geothermometer [33]. The metamorphic ages of corundum-bearing garnet–sillimanite gneisses are constrained to be ca. 1.95–1.83 Ga, which recorded a clockwise *P*–*T* path with peak metamorphic conditions of ~890–940 °C at ~7.5–9.8 kbar [34]. Wang et al. (2023) [35] obtained a clockwise *P*–*T* path with the peak metamorphic condition of 948–1048 °C/11–14 kbar, and metamorphic ages of ca. 1.96–1.86 Ga for mafic granulites.

The Boluositanmiao Complex is mainly composed of felsic gneisses, and the protolith crystallization ages of these felsic gneisses are determined at ca. 1.84–1.82 Ga [30,48,49].

In the Bayanwulashan Complex, there are felsic gneisses, amphibolites and metasedimentary rocks [28,36,37,42,48,50,51]. Zircon U–Pb dating indicates that the crystallization age for the protolith of felsic gneisses is ca. 2.40 to 2.23 Ga [48,50], whereas the metamorphic ages of these rocks have been constrained to be ca. 1.96–1.77 Ga [28,36,37]. The crystallization ages for the protolith of amphibolites were dated at ca. 2.30–2.34 Ga, which have metamorphic ages of ca. 1.94–1.80 Ga [36,51]. The detrital zircons from metasedimentary rocks (e.g., felsic paragneiss) range from ca. 2.50 to 2.27 Ga, which underwent ca. 1.90–1.80 Ga metamorphism [36,42]. These late Paleoproterozoic metamorphic ages in the Diebusige and Bayanwulashan Complexes indicate that the Alxa Block may be the westward extension of the KB [27,30,33–35].

3. Analytical Methods

The mineral compositions (Tables S1–S3) were analyzed using the JEOL JXA-8230 electron microprobe (EMP) at the State Key Laboratory of Continental Dynamics (SKLCD), Northwest University, Xi'an. The operating conditions are a 15 kV accelerating voltage, a beam current of 10 nA, and a beam diameter of 2 μm.

The whole-rock compositions were determined by X-ray fluorescence (XRF) analyses (Table 1) at the SKLCD, Northwest University, Xi'an. The FeO compositions were measured by a titration method at the Regional Geology and Mineral Resources Institute, Langfang, Hebei province.

Separated zircon grains were mounted in epoxy resin and polished to expose grain centers. Cathodoluminescence (CL) imaging was carried out at Tuoyan Analytical Technology Co., Ltd., Guangzhou, which was used to identify internal structures of zircons. Zircon U–Pb dating and rare earth element (REE) analysis were simultaneously carried out by using laser ablation inductively coupled plasma mass spectrometry (LA-ICP-MS) at the Wuhan Sample Solution Analytical Technology Co., Ltd., Wuhan, China. The laser spot was 24 μm in size, and a laser frequency of 5 Hz was used. Harvard zircon 91500 and glass NIST610 were selected as external standards. Detailed operating conditions, analytical procedures, and data processing methods can be found in Liu et al. (2010) [52].

4. Field Occurrence and Petrology

4.1. Field Occurrence

The Diebusige and Bayanwulashan Complexes mainly comprise felsic gneiss with amphibolite lenses or interlayers (Figure 2a,b). Amphibolites display a homogeneous distribution of leucosomes (Figure 3a,e,f), suggesting they have experienced partial melting (Figure 3a–f). Amphibolite samples ALS2164 and ALS2166 were collected from the Diebusige Complex, whereas amphibolite samples ALS2191 and ALS2156 are from the Bayanwulashan Complex. Detailed petrography and mineral chemistry were carried out for three amphibolite samples (i.e., ALS2164, ALS2166 and ALS2191).

4.2. Petrology and Mineral Chemistry

Petrographic features are showed in Figures 4 and 5, whereas classifications of mineral composition are presented in Figure 6. The mineral abbreviations in this study follow Whitney and Evans (2010) [53]. Hornblende compositions are plotted on the Leake classification diagram [54].

4.2.1. Amphibolite Sample ALS2164

Amphibolite sample ALS2164 displays a porphyroblastic texture and is composed of clinopyroxene (~15%), plagioclase (~45%), hornblende (~30%), K-feldspar (~8%), minor quartz (~2%), with accessory zircon, apatite, ilmenite and hematite (Figure 4a–f). Plagioclase occurs as coarse-grained crystals and is in textural equilibrium with clinopyroxene, hornblende and K-feldspar (Figure 4a–f). Minor quartz appears as interstitial crystals between hornblende and clinopyroxene (Figure 4e,f). Ilmenite and hematite are present as interstitial grains (Figure 4d,e). Clinopyroxenes are diopside in composition (Table S1; Figure 6a). Plagioclases have X_{An} of 0.32–0.34 and are andesine in composition (Table S1; Figure 6b). Hornblendes are pargasite and magnesio-hastingsite in composition, with Ti = 0.22–0.28 cpfu. and X_{Mg} = 0.60–0.62 (Table S1; Figure 6d).

4.2.2. Amphibolite Sample ALS2166

Amphibolite sample ALS2166 is composed of clinopyroxene (~15%), plagioclase (~55%), hornblende (~30%) with accessory ilmenite, apatite and zircon (Figure 4g,h). Ilmenite is present as interstitial grains (Figure 4g,h). Clinopyroxenes in this sample are diopside in composition (Table S2; Figure 6a), which are similar to those of clinopyroxene from sample ALS2164. Plagioclases display andesine composition with homogeneous X_{An} value (0.34–0.37) (Table S2; Figure 6b). Coarse-grained hornblendes are ferropargasite or pargasite, with X_{Mg} values of 0.45–0.49 and Ti contents of 0.20–0.29 cpfu. (Table S2; Figure 6d).

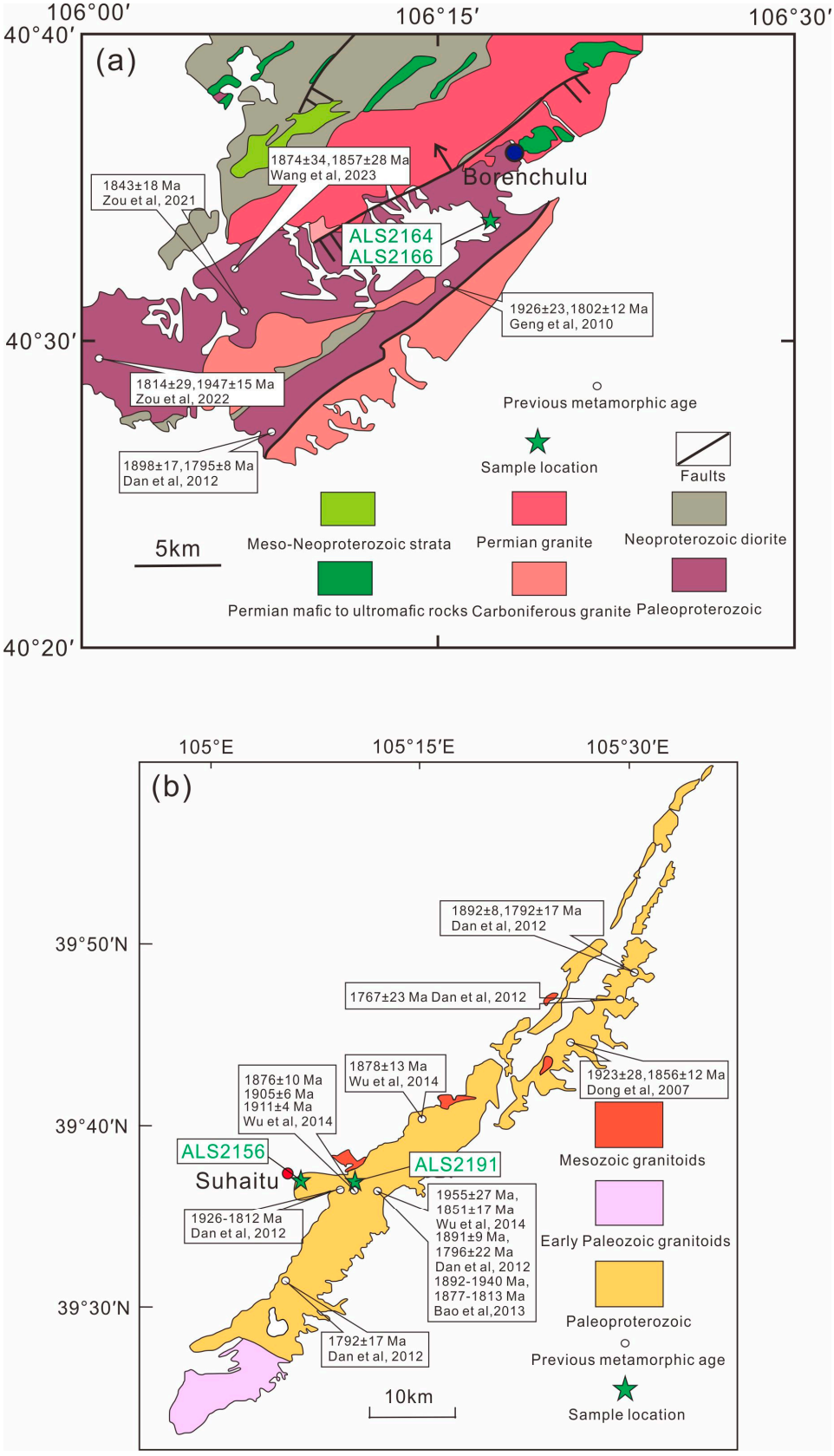

Figure 2. Geological maps of the Diebusige Complex [29,33–36] (**a**) and the Bayanwulashan Complex [28,36,37,51] (**b**) in the Alxa Block (revised from BGMRIM (1991) [38]).

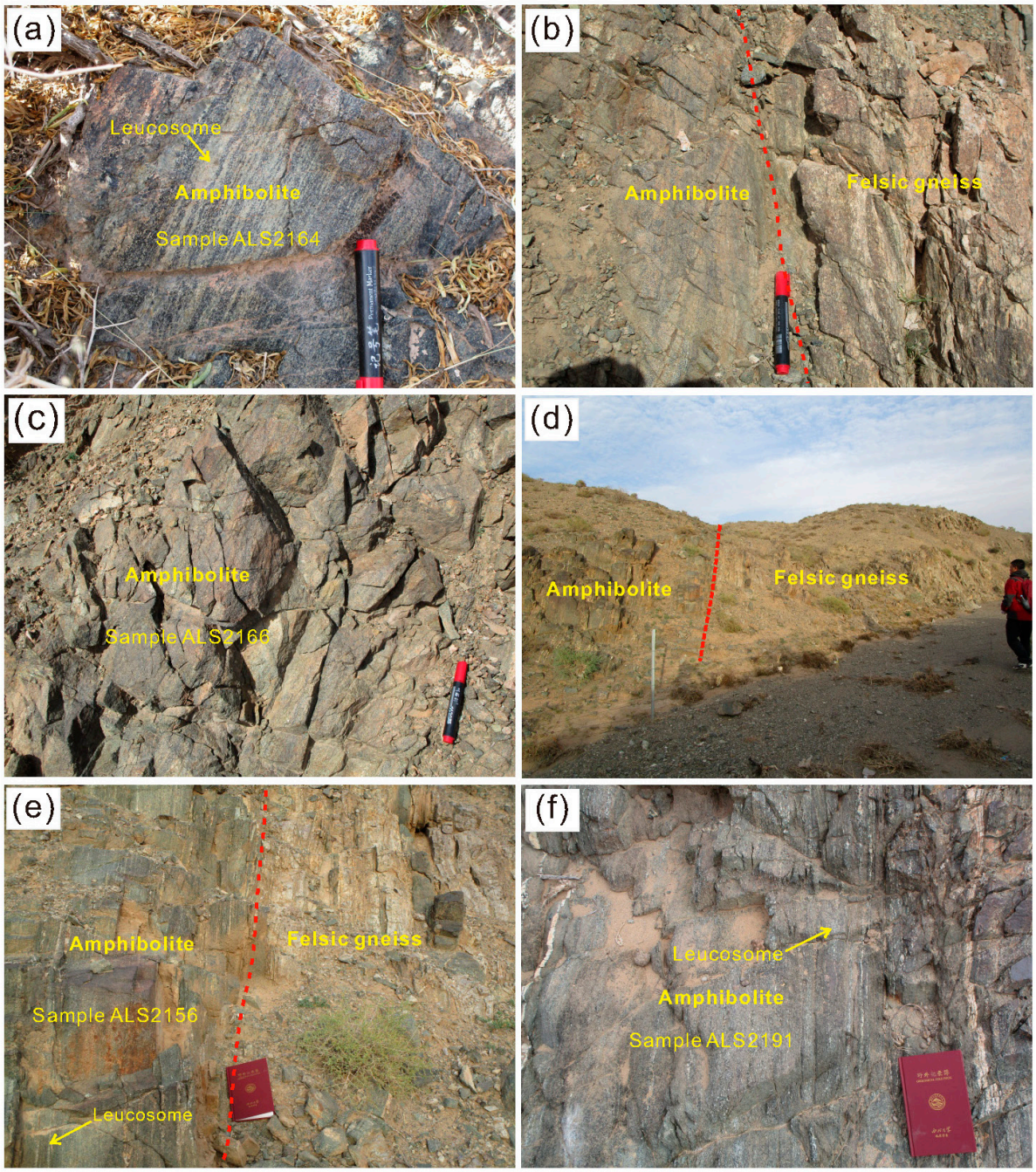

Figure 3. Field photographs of the amphibolites: (**a**–**c**) amphibolite interlayers and felsic gneiss in the Diebusige Complex; (**d**–**f**) amphibolite interlayers and felsic gneiss in the Bayanwulashan Complex.

4.2.3. Amphibolite Sample ALS2191

Amphibolite sample ALS2191 consists of clinopyroxene (~10%), plagioclase (~47%), hornblende (~40%), K-feldspar (~2%) and minor quartz (~3%), with accessory ilmenite, sphene and zircon (Figure 5a–d). Clinopyroxene, hornblende, plagioclase and quartz are in contact with each other. Clinopyroxene grains have been transformed to the composite of quartz and actinolite, which was termed as pseudomorph of Cpx (Figure 5a–d). This phenomenon has been observed in clinopyroxene from HP–HT metamorphic rocks, which was considered to be formed by retrogression with water ingress [55–61]. K-feldspar was observed as veins in the fractures (Figure 5b), which may be crystallized from K-bearing fluid during retrogression. Ilmenite is present as interstitial grains (Figure 5a).

Sphene occurs as corona around ilmenite (Figure 5f). Plagioclases have slight compositional variation with X_{An} = 0.36–0.39 and belong to andesine (Figure 6b; Table S3). Hornblendes belong to pargasite and magnesio-hastingsite, with X_{Mg} values of 0.50–0.52 and Ti contents of 0.18–0.31 (Figure 6d; Table S3), whereas actinolites have higher X_{Mg} values of 0.62–0.72 but lower Ti contents of 0.00–0.03 (Figure 6c; Table S3).

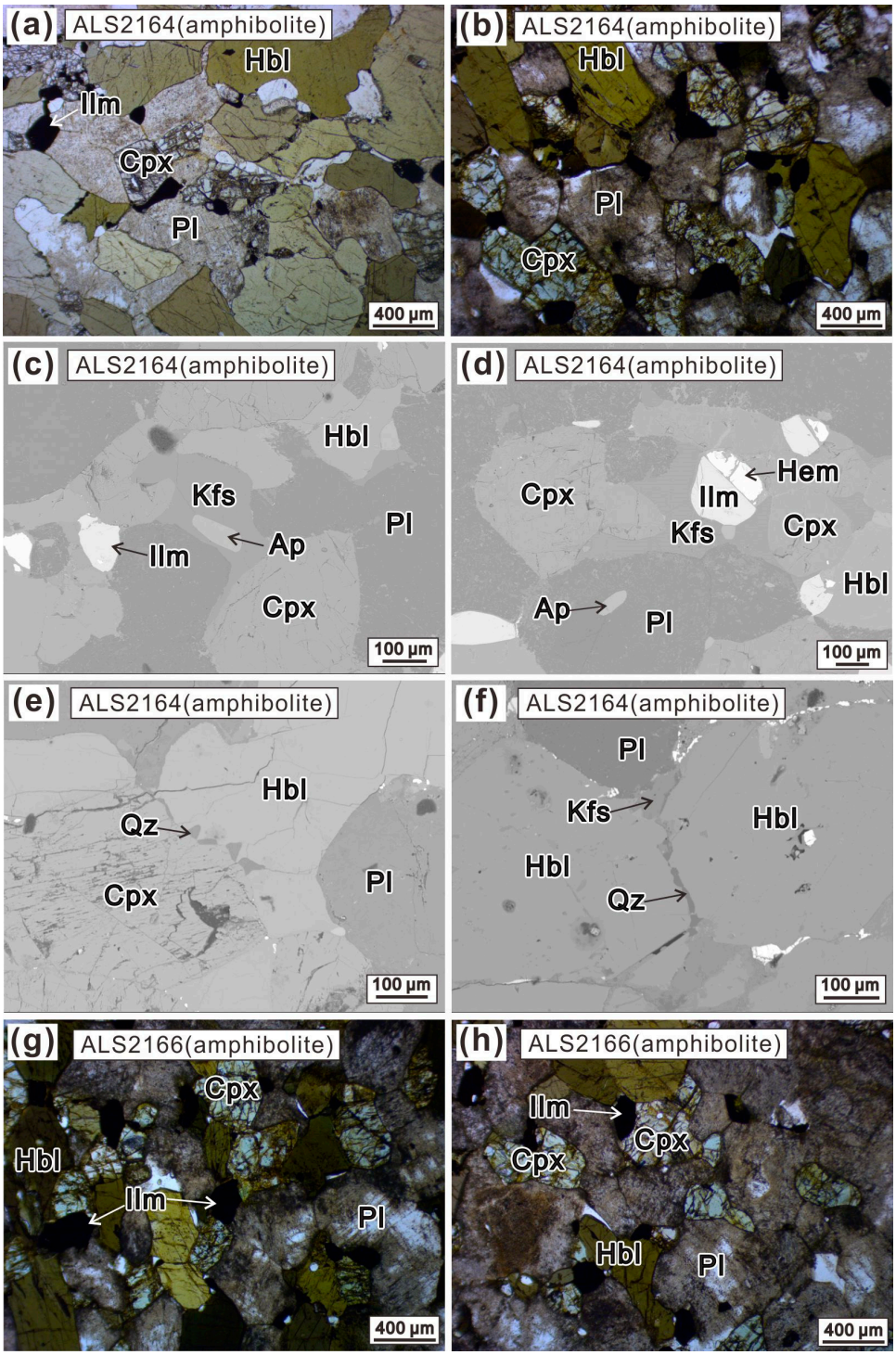

Figure 4. Photomicrographs for the amphibolite samples ALS2164 and ALS2166 in the Diebusige Complex: (**a**,**b**) clinopyroxene, hornblende, plagioclase and ilmenite (plane polarized light); (**c**–**f**) back-scattered electron (BSE) image shows K-feldspar, quartz, apatite, ilmenite and hematite; (**g**,**h**) clinopyroxene, hornblende and plagioclase (plane polarized light).

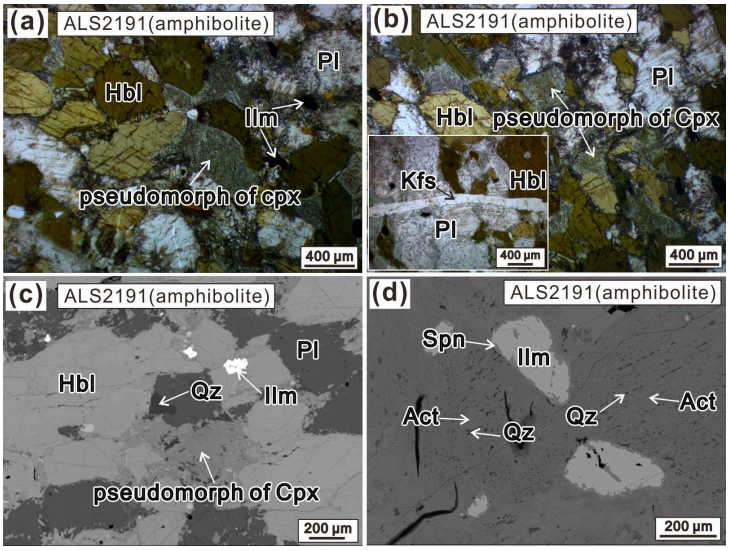

Figure 5. Photomicrographs for the amphibolite sample ALS2191 in the Bayanwulashan Complex: (**a**,**b**) hornblende, plagioclase, K-feldspar and pseudomorph of clinopyroxene (plane polarized light); (**c**,**d**) BSE image shows quartz, sphene, and actinolite and quartz in the pseudomorph of clinopyroxene.

4.3. Mineral Assemblage Evolution

Based on observations of field outcrops and petrography described above, the peak mineral assemblage of cpx + hbl + pl + kfs + qz + ilm + melt is identified for sample ALS2164, and the peak mineral assemblage of cpx + hbl + pl ± kfs + ilm + qz + melt is inferred for sample ALS2191. Actinolites in the pseudomorph of Cpx (Figure 5d; sample ALS2191) are a typical greenschist facies mineral, indicating later hydrothermal alteration. Sphenes only occur around ilmenite in the pseudomorph of Cpx and have not been found in the other domain (i.e., Figure 5a,c). Likely, sphene coronas around ilmenite in the pseudomorph of Cpx (Figure 5d; sample ALS2191) are also the product of hydrothermal alteration.

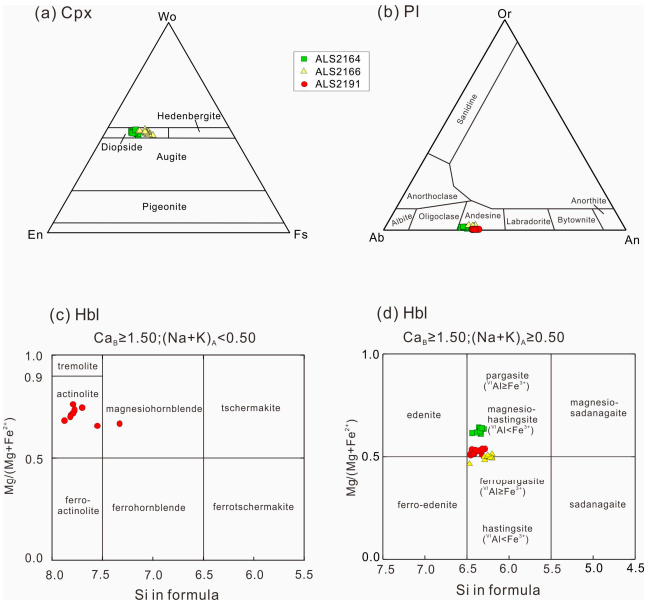

Figure 6. Compositions of clinopyroxene, plagioclase and hornblende: (**a**) the Wo–En–Fs classification diagram for the clinopyroxene; (**b**) the X_{Or}–X_{Ab}–X_{An} diagram for the plagioclase; (**c**,**d**) the classification diagram for the hornblende.

5. Calculation of Metamorphic Conditions

5.1. Phase Equilibrium Modelling

Phase equilibrium modelling was carried out for amphibolite samples ALS2191 and ALS2164 in the system NCKFMASHTO (Na_2O–CaO–K_2O–FeO–MgO–Al_2O_3–SiO_2–H_2O–TiO_2–O_2) using the Theriak-Domino software (ver.11.03.2020; [62]), with the dataset file ds62_mafic (adopted from the Thermocalc database ds62 by Holland and Powell, 1998 [63], 2011 [64]). The adopted activity–composition (a–x) models are listed in the following: liquid (melt), clinopyroxene and hornblende [65]; garnet and orthopyroxene [66]; olivine [64]; plagioclase [67]; magnetite–spinel [68]; and ilmenite–hematite [69]. Pure phases include quartz and rutile. The amount of FeO was analyzed by titration and then Fe_2O_3 was calculated by the difference. The T–X_{H2O} pseudosection was used to evaluate the appropriate H_2O content for the final P–T pseudosection modelling. The bulk-rock compositions for modelling are listed in Table 1.

5.1.1. Amphibolite Sample ALS2164

A T–X_{H2O} pseudosection constructed at 8 kbar (Figure 7a) using the oxygen content obtained by the Fe^{2+} titration was used to select a suitable H_2O content, so that the final retrograde mineral assemblage is stable just above the post-melt-loss solidus [70]. The adopted pressure of 8 kbar is consistent with the pressure range for the peak mineral assemblage of cpx–hbl–pl–kfs–qz–ilm–liq in the P–T pseudosection (Figure 7b). The variations in X_{H2O} correspond to a range of H_2O contents from 0 to 5 mol.% (Table 1; Figure 7b,c). A X_{H2O} value of 0.65 (equivalent to 3.25 mol.% H_2O) was chosen, which crosses the liquid-out line of the peak mineral assemblage (Table 1; Figure 7b).

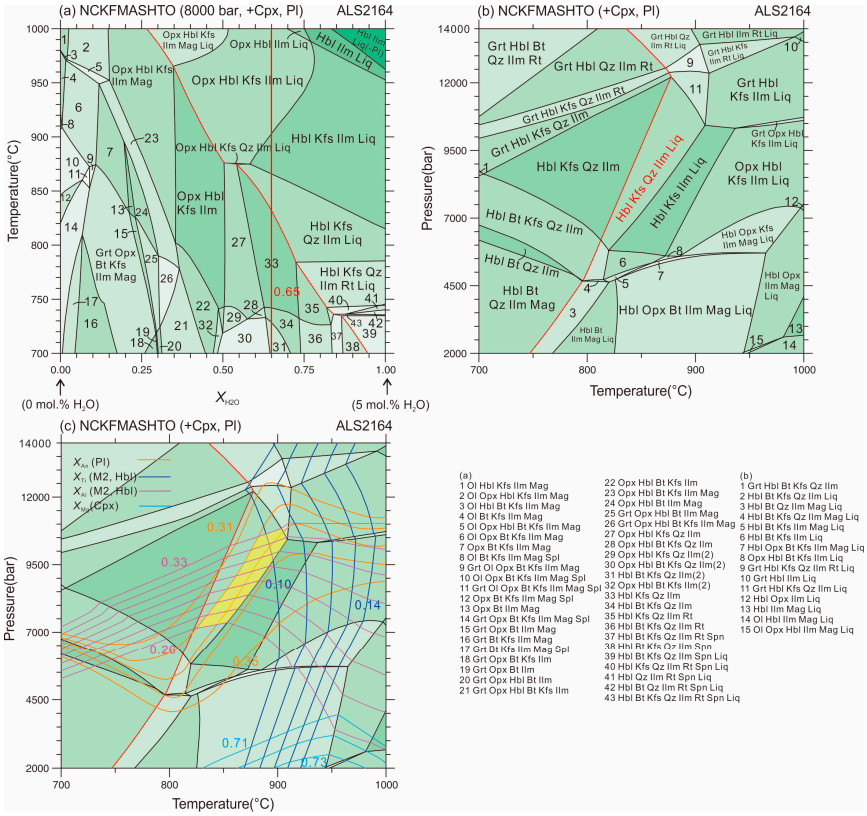

Figure 7. T–X_{H2O} and P–T pseudosections for the amphibolite sample ALS2164 in the Diebusige Complex: (**a**) T–X_{H2O} pseudosection at 8 kbar; (**b**) P–T pseudosection; (**c**) P–T pseudosection with isopleths of X_{Ti}(M2) and X_{Al}(M2) in hornblende, X_{Mg} in clinopyroxene and X_{An} in plagioclase. The field of peak mineral assemblage is marked by cpx + hbl + pl + kfs + ilm + liq in red type. Red bars in (**a**) denote H_2O content used for subsequent modelling.

The *P*–*T* pseudosection was calculated over the *P*–*T* window of 2–14 kbar/700–1000 °C (Figure 7b). The *P*–*T* pseudosection is presented with isopleths of X_{Ti}(M2) and X_{Al}(M2) in hornblende, X_{Mg} in clinopyroxene and X_{An} in plagioclase (Figure 7c). The inferred peak mineral assemblage of cpx + hbl + pl + kfs + qz + ilm + liq was stable over a *P*–*T* range of 810–910 °C/5.8–12.2 kbar (Figure 7b). The peak metamorphic condition is furtherly constrained to be 825–910 °C/7.2–10.8 kbar by the measured X_{An} = 0.32–0.34 of plagioclase and X_{Al}(M2) = 0.26–0.33 of hornblende (Figure 7c). However, the measured X_{Ti}(M2) of 0.11–0.14 in hornblende and X_{Mg} of 0.74–0.80 in clinopyroxene fall outside of the range of the peak phase field (Table S1; Figure 7c).

5.1.2. Amphibolite Sample ALS2191

The H_2O content was determined using the *T*–X_{H2O} pseudosection (Figure 8a) to ensure that the final mineral assemblage is stable just above the solidus [70]. The *T*–X_{H2O} pseudosection was constructed at 9 kbar, which is within pressure range for the peak assemblage of cpx–hbl–pl–kfs–qz–ilm–liq in the *P*–*T* pseudosection (Figure 8b). The variations in X_{H2O} correspond to a range of H_2O contents from 0 to 5.0 mol.% (Table 1; Figure 8a). The peak mineral assemblage of cpx–hbl–pl–kfs–qz–ilm–liq occurs at >0.55 X_{H2O} and 772–868 °C in the *T*–X_{H2O} pseudosection (Figure 8a). A X_{H2O} value of 0.64 (equivalent to 3.20 mol.% H_2O) was selected for the subsequent *P*–*T* pseudosection calculation, which crosses the liquid-out line for the peak mineral assemblage (Table 1; Figure 8a).

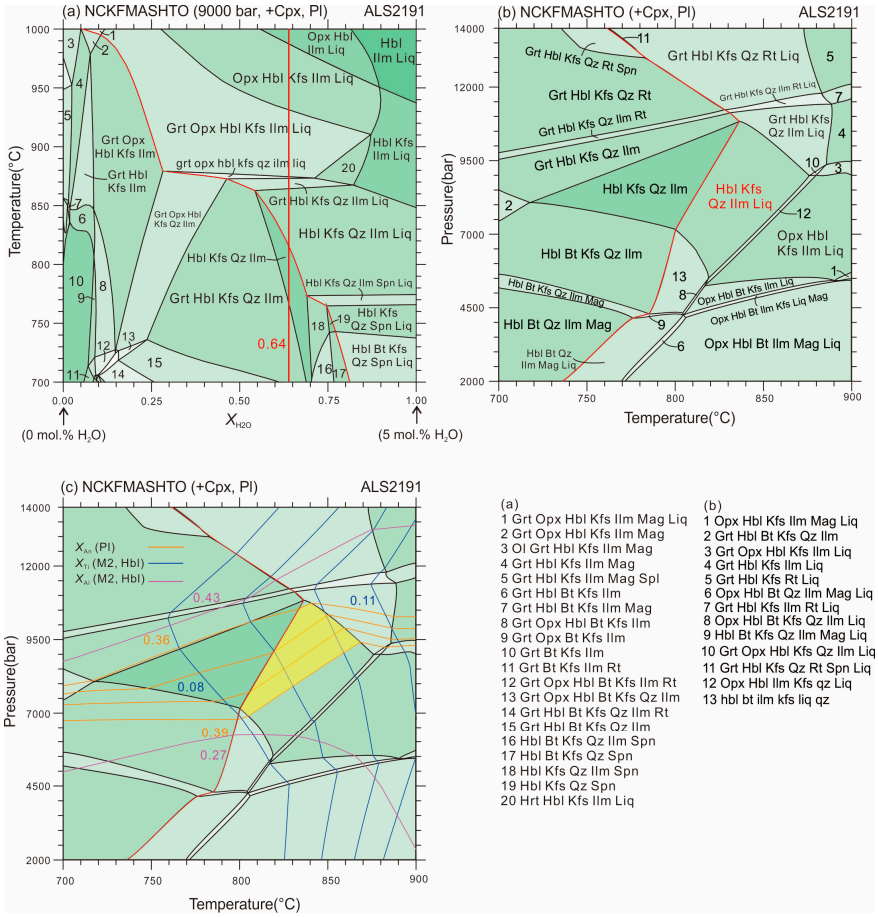

Figure 8. *T*–X_{H2O} and *P*–*T* pseudosections for the amphibolite sample ALS2191 in the Bayanwulashan Complex: (**a**) *T*–X_{H2O} pseudosection at 9 kbar; (**b**) *P*–*T* pseudosection; (**c**) *P*–*T* pseudosection with isopleths of X_{Ti}(M2) and X_{Al}(M2) in hornblende, and X_{An} in plagioclase. The field of peak mineral assemblage is marked by cpx + hbl + pl + kfs + qz + ilm + liq in red type. Red bars in (**a**) denote H_2O content used for subsequent modelling.

The *P–T* pseudosection was calculated over the *P–T* window of 700–900 °C and 2–14 kbar (Figure 8c). The solidus was modelled at temperature between 737 and 837 °C. Isopleths of X_{Ti}(M2) and X_{Al}(M2) in hornblende, and X_{An} in plagioclase, were contoured on the fields of relevant assemblages in the *P–T* pseudosection (Figure 8c). The inferred peak mineral assemblage of cpx + pl ± kfs + hbl + ilm + qz + liq occurs in the range of 5.5–10.8 kbar/800–877 °C (Table S1; Figure 8b). The measured X_{An} = 0.36–0.39 of plagioclase furtherly constrained the peak metamorphic condition to be 800–870 °C/7.0–10.7 kbar. As the X_{Al}(M2) in hornblende ranges from 0.27 to 0.43 (Figure 8c; Table S3), it cannot furtherly constrain the *P–T* condition of the peak metamorphism. Hornblendes have a high X_{Ti}(M2) of 0.09–0.16, of which the Ti-rich composition (X_{Ti}(M2) = 0.11–0.16) of hornblende (Table S3) and the corresponding X_{Ti}(M2) isopleths fall outside of the field of the peak mineral assemblage.

Table 1. Bulk compositions used for phase equilibrium modelling.

Whole Rock Compositions (wt.%)													
Sample	**SiO_2**	**TiO_2**	**Al_2O_3**	**Fe_2O_3**	**FeO**	**MnO**	**MgO**	**CaO**	**Na_2O**	**K_2O**	**P_2O_5**	**LOI**	**Total**
ALS2164	45.23	2.35	11.85	6.36	7.21	0.19	8.81	10.38	2.53	1.76	0.65	1.49	99.61
ALS2191	48.65	1.27	14.76	3.32	7.75	0.17	6.38	9.49	2.78	2.10	0.44	1.66	99.63
Normalized Molar Proportion Used for Phase Equilibria Modelling													
	Figures			**H_2O**	**SiO_2**	**Al_2O_3**	**CaO**	**MgO**	**FeO**	**K_2O**	**Na_2O**	**TiO_2**	**O**
ALS2164	Figure 7a	x = 0		0.00	48.07	7.42	10.84	13.96	11.49	1.19	2.61	1.88	2.54
		x = 1		5.00	45.66	7.05	10.30	13.26	10.92	1.13	2.48	1.78	2.41
	Figure 7b,c			3.25	46.51	7.18	10.49	13.50	11.12	1.15	2.52	1.82	2.46
ALS2191	Figure 8a	x = 0		0.00	53.10	9.49	10.42	10.38	9.80	1.46	2.94	1.04	1.36
		x = 1		5.00	50.45	9.02	9.90	9.86	9.31	1.39	2.79	0.99	1.29
	Figure 8b,c			3.20	51.40	9.19	10.09	10.05	9.48	1.42	2.85	1.01	1.32

Abbreviation: LOI, loss on ignition.

5.2. Conventional Thermobarometry

Hbl–pl–qz thermobarometry [71,72] yielded metamorphic *PT* conditions of 777 °C/3.0 kbar–785 °C/4.0 kbar, 732 °C/6.6 kbar–810 °C/6.7 kbar and 738 °C/6.1 kbar–759 °C/3.0 kbar for samples ALS2164, ALS2166 and ALS2191, respectively. Ti-in-amphibole thermometry [73] yielded temperatures of 825–881 °C (an average of 861 °C), 808–917 °C (an average of 866 °C) and 783–913 °C (an average of 851 °C) for samples ALS2164, ALS2166 and ALS2191, respectively (Tables S1–S3; Figure 9a). The revised Ti-in-zircon thermometry was also used to estimate the metamorphic temperatures [74]. The coexisting Ti-phase in our samples is ilmenite, which means the TiO_2 activity was 0.6 [75]. The SiO_2 activity was set as 1.0 due to the presence of quartz. After excluding abnormal spot >20 ppm that may be caused by Ti-rich mineral inclusions, the metamorphic temperatures recorded by zircons were estimated to be 679–850 °C with a mean value of 763 °C (2.80–16.0 ppm), 728–857 °C with a mean value of 780 °C (4.96–17.40 ppm), and 689–853 °C with a mean value of 768 °C (3.15–16.80 ppm), for samples ALS2164, ALS2166 and ALS2191, respectively (Table S4; Figure 9b).

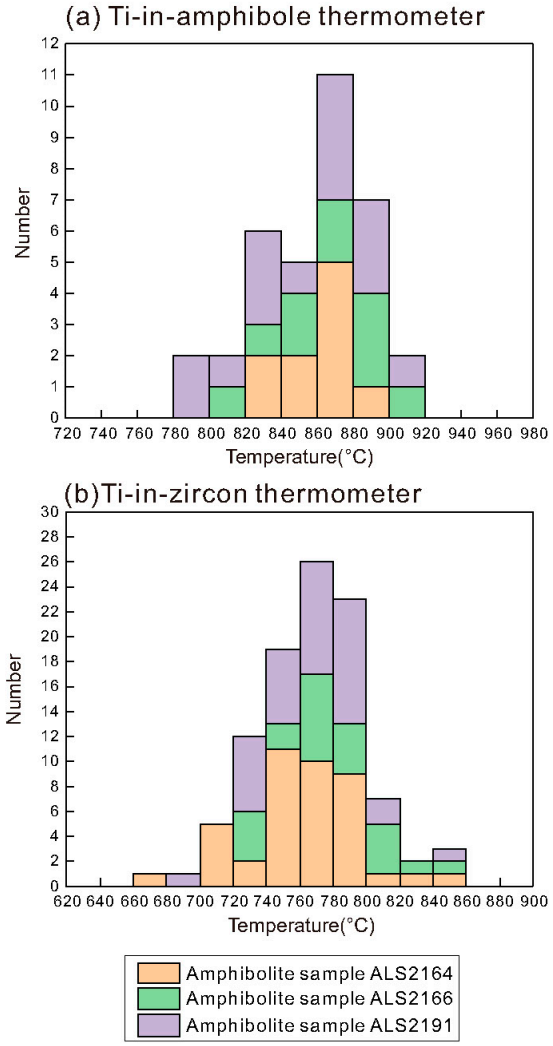

Figure 9. Metamorphic temperatures calculated for amphibolite samples ALS2164, ALS2166 and ALS2191 using Ti-in-amphibole (**a**) and Ti-in-zircon (**b**) thermometers.

6. Zircon U–Pb Dating

6.1. Amphibolite Sample ALS2164

Zircon grains from this sample are rounded or stubby in shape, with a size of 100–200 μm, and exhibit planar or no zoning, indicating metamorphic origin (Figure 10). Fifty-three spot analyses were conducted on metamorphic zircons, of which fifty-two spot analyses were plotted on or close to the concordia curve (Figure 11a). After excluding twelve spots with old apparent data (may be carried out on inherited igneous zircons), the remaining concordant data yielded a weighted mean $^{207}Pb/^{206}Pb$ age of 1847 ± 25 Ma (n = 40, MSWD = 1.4) (Table S4; Figure 11a). On the chondrite-normalized REE patterns (data of chondrite are cited from Sun and McDonough (1989) [76]), all zircons show variable Eu anomalies (Eu/Eu* = 0.25–6.02) and an enriched HREE pattern ($(Gd/Lu)_N$ = 0.02–0.08) (Table S5; Figure 11b). Th vs U diagram (Figure 11b) displays relatively low Th (27.91–221.54 ppm) and high U (31.48–268.31 ppm) contents with Th/U ratios of 0.45–2.41 (Figure 11b; Table S4).

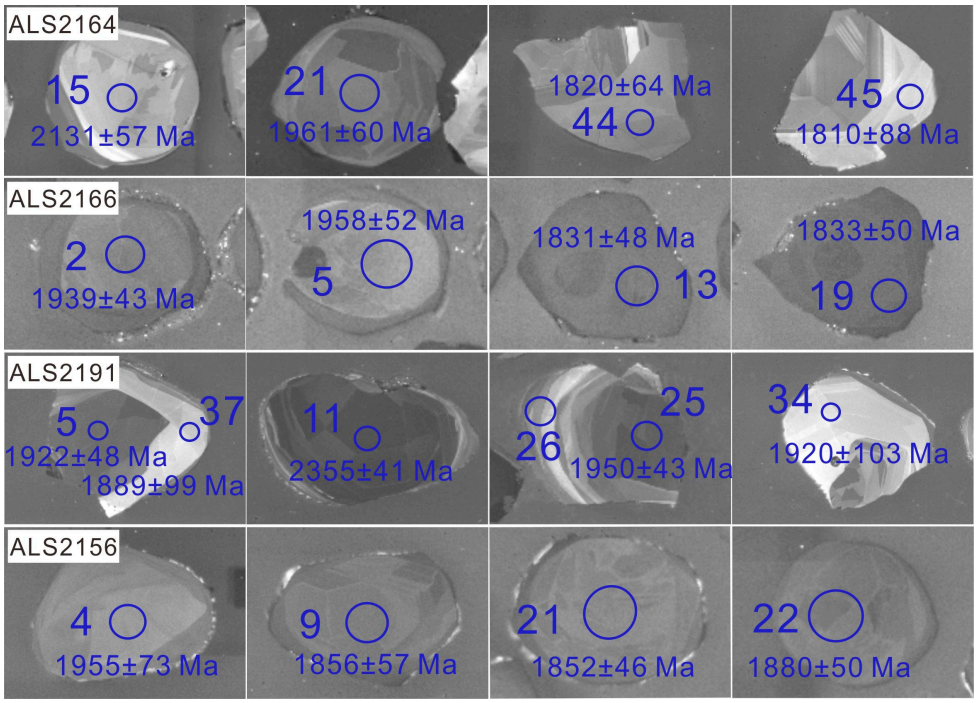

Figure 10. CL images of representative zircons within amphibolite samples ALS2164, ALS2166, ALS2191 and ALS2156. The blue circles represent analytical spot with a size of ~24 μm.

6.2. Amphibolite Sample ALS2166

Zircon grains from this sample are generally stubby to rounded in shape, with a diameter of 70–150 μm. Features under CL images suggest they are metamorphic rather than igneous in origin (Figure 10). Twenty-three spot analyses were performed on metamorphic zircons, and all spot analyses yielded concordant data (Table S4). These concordant data yielded a weighted mean $^{207}Pb/^{206}Pb$ age of 1817 ± 21 Ma Ma (n = 23, MSWD = 2.0) (Figure 11c). Obviously, all zircons exhibit variable Eu anomalies (Eu/Eu* = 0.26–1.19) and an enriched HREE pattern ($(Gd/Lu)_N$ = 0.01–0.03) (Figure 11d; Table S5). The Th vs U diagram displays that all zircons have relatively low Th (68.58–244.17 ppm) and high U (268.19–811.76 ppm) contents with low Th/U ratios (0.24–0.44) (Figure 11d).

6.3. Amphibolite Sample ALS2191

Zircon grains from this sample are rounded or stubby in shape, with a diameter of 100–200 μm, and display sector and patchy zoning, reflecting metamorphic origin (Figure 10). Forty spot analyses were performed on metamorphic zircons, of which thirty-eight spot analyses yielded concordant data (Table S4). After excluding three old apparent age of 2355 ± 41, 2300 ± 39 and 2080 ± 68 Ma (i.e., spots 3, 4 and 11), the remaining concordant data yielded a weighted mean $^{207}Pb/^{206}Pb$ age of 1901 ± 22 Ma (n = 35, MSWD = 0.4) (Table S4; Figure 11e). Notably, all metamorphic zircons display an enriched HREE pattern ($(Gd/Lu)_N$ = 0.02–0.08) with negative Eu anomalies (Eu/Eu* = 0.13–0.60)(Table S5; Figure 11f)). The U vs Th diagram shows that metamorphic zircons have relatively low Th (66.83–714.27 ppm) and high U (25.03–791.68 ppm) contents, with variable Th/U ratios (0.38–4.82) (Figure 11f; Table S4).

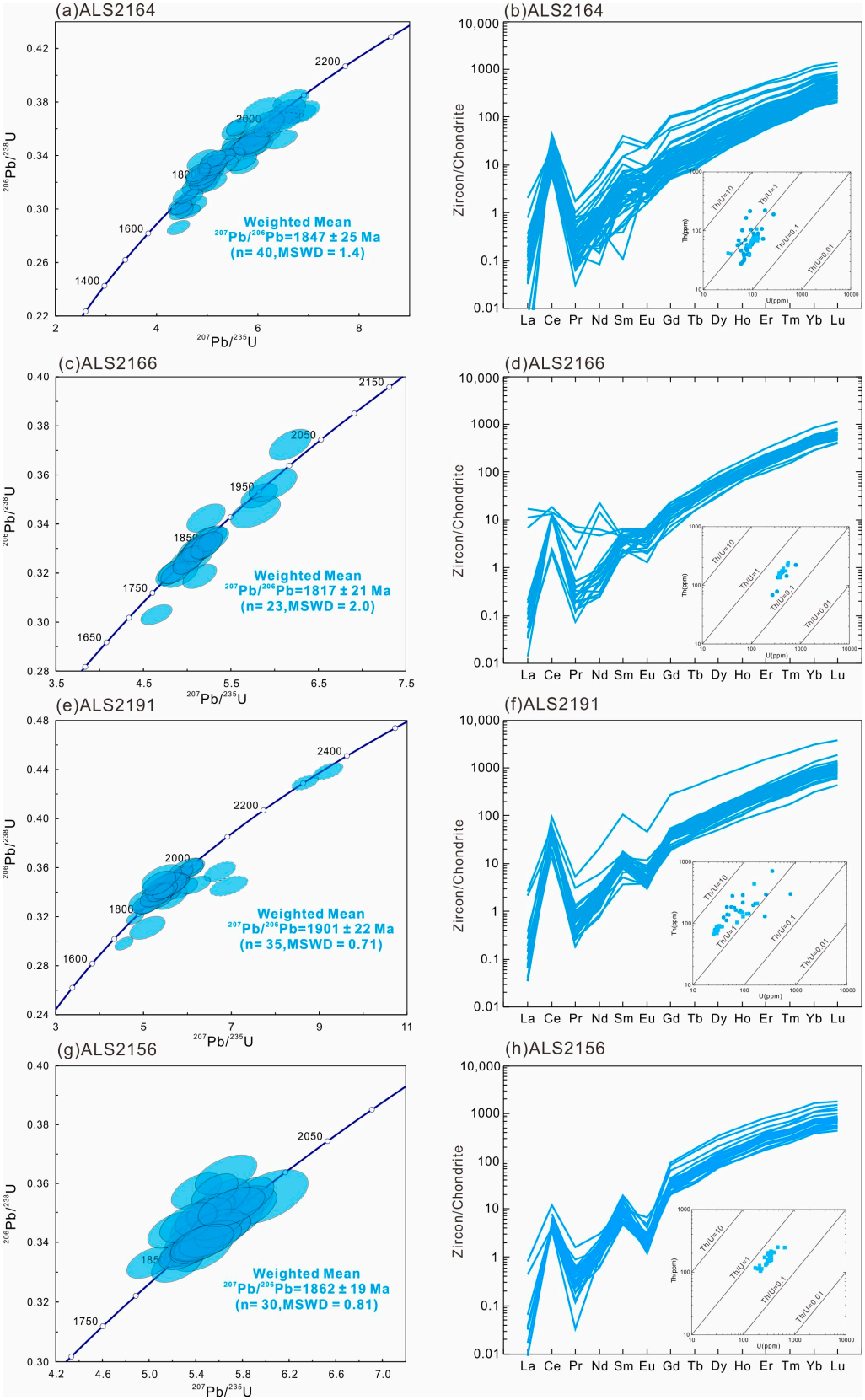

Figure 11. Concordia diagrams, chondrite-normalized rare earth element patterns and Th vs. U diagram with Th/U isopleths for the metamorphic zircons of amphibolite samples ALS2164 (**a**,**b**), ALS2166 (**c**,**d**), ALS2191 (**e**,**f**) and ALS2156 (**g**,**h**).

6.4. Amphibolite Sample ALS2156

Zircon grains from this sample are stubby to rounded in shape, with a size of 60–120 μm, and display fir-tree or patchy zoning, suggesting metamorphic origin (Figure 10). All thirty spot analyses on metamorphic zircons yielded concordant data (Table S4). These concordant data yielded a weighted mean $^{207}Pb/^{206}Pb$ age of 1862 ± 19 Ma (n = 30, MSWD = 0.81) (Table S4; Figure 11g). On the chondrite-normalized REE patterns (Figure 11h), all zircons display a enriched heavy REE pattern ($(Gd/Lu)_N$ = 0.02–0.06) with negative Eu anomalies (Eu/Eu* = 0.06–0.38) (Table S5; Figure 11h). The U versus (vs.) Th diagram shows that all zircons have relatively low Th (104.69–251.08 ppm) and high U (172.68–645.94 ppm) contents, with low Th/U ratios (0.38–0.68) (Table S4; Figure 11h).

7. Discussion

7.1. Age Interpretation of Amphibolites

In the eastern Alxa Block, a large number of metamorphic ages have been reported in the Bayanwulashan and Diebusige Complexes [19,20,24,25,30,31,34,41,45]. For example, SHRIMP and LA-ICP-MS zircon U–Pb dating yielded two metamorphic age groups of 1.95–1.90 Ga and 1.85–1.80 Ga for granitic gneiss and amphibolites from the Bayanwulashan Complex [19,45]. Wu et al. (2014) [31] reported two groups of metamorphic ages of 1.95–1.90 Ga and 1.85–1.80 Ga by LA-ICP-MS zircon U–Pb dating for several orthogneiss samples in the Bayanwulashan Complex. Additionally, SIMS zircon U–Pb dating determined that orthogneisses and paragneisses from both the Diebusige and Bayanwulashan Complexes recorded two groups of metamorphic ages of ca. 1.90 Ga and ca. 1.80 Ga [30]. In the Diebusige Complex, Geng et al. (2007, 2010) [34,35] constrained the timing of metamorphism of felsic gneiss to be ca. 2.00–1.90 Ga and ca. 1.93 Ga, respectively. Recently, Zou et al. (2021) [24] demonstrated that the granulite-facies metamorphism of magnetite quartzite from the Diebusige Complex occurred at ca. 1.85 Ga by LA-ICP-MS zircon U–Pb dating. Moreover, a corundum-bearing garnet–sillimanite gneiss sample from the Diebusige Complex was determined to firstly undergo granulite-facies metamorphism at ca. 1.95 Ga, then achieved UHT metamorphic condition, and finally cooled to the solidus at ca. 1.83 Ga [25]. Wang et al. (2023) [35] reported metamorphic ages of ca. 1.96–1.86 Ga for UHT mafic granulites in the Diebusige Complex. Therefore, both the Bayanwulashan and Diebusige Complexes underwent metamorphism at ca. 1.95–1.90 Ga and ca. 1.85–1.80 Ga.

In this study, LA-ICP-MS zircon U–Pb dating yielded four weighted mean $^{207}Pb/^{206}Pb$ ages of 1847 ± 25, 1817 ± 21, 1901 ± 22 and 1862 ± 19 Ma for metamorphic zircons of amphibolite samples ALS2164, ALS2166, ALS2191 and ALS2156, respectively (Figure 11). These metamorphic chronological data (ca. 1901–1817 Ma) are consistent with reported zircon U–Pb ages in the Alxa Block (Table S6). The calculated average values of Ti-in-zircon temperatures of 763, 768 and 780 °C suggest that the amphibolite-facies metamorphism occurred at ca. 1901–1817 Ma.

7.2. Metamorphic Style and Tectonic Implications

Metamorphic conditions calculated by *P–T* pseudosection modelling and hbl–pl–qz thermobarometry in this study, and previous results in the Alxa Block, are summarized in Figure 12, in which the boundaries of metamorphic facies are from Brown (2014) [9]. As described in Section 5.1, the metamorphic *P–T* conditions of 825–910 °C/7.2–10.8 kbar were obtained for amphibolite sample ALS2164, whereas that of 800–870 °C/7.0–10.7 kbar were constrained for amphibolite sample ALS2191. The dated zircons display the relatively low crystallization temperatures with averages of 763 °C, 768 °C and 780 °C, which are consistent with the metamorphic temperatures constrained by the hbl–pl–qz thermobarometry in Figure 12. In addition, the Ti-in-amphibole thermometer yielded high metamorphic temperatures with averages of 861 °C, 866 °C and 851 °C, which agree with the peak metamorphic temperatures constrained by *P–T* pseudosection modelling (Figure 12). Our samples preserved typical amphibolite-facies mineral assemblage (Opx-free mineral assemblage), which are consistent with temperature and pressure estimates from hbl–pl–qz

thermobarometry and the Ti-in-zircon thermometer. Such a large difference in metamorphic conditions calculated by different methods may be a result of the following reasons: (1) The absolute *PT* conditions of the *P–T* pseudosection modelling may have a large error (~0.1 GPa and ~50 °C; [77,78]). Thus, considering this uncertainty range, the results obtained from conventional thermobarometry can closely align with those derived from *P–T* pseudosection modelling. (2) These amphibolites may have experienced granulite-facies metamorphism although they are characterized by opx-free mineral assemblage. This can be attributed to the effect of bulk-rock composition, as interpreted by opx-bearing phase fields occur at high temperatures in these samples (Figures 7 and 8). Nevertheless, the lower limit of metamorphic conditions constrained by *P–T* pseudosection modelling are consistent with the upper limit of metamorphic conditions yielded by the hbl–pl–qz thermobarometer (732–810 °C/3.0–6.7 kbar) in uncertainty (Figure 12).

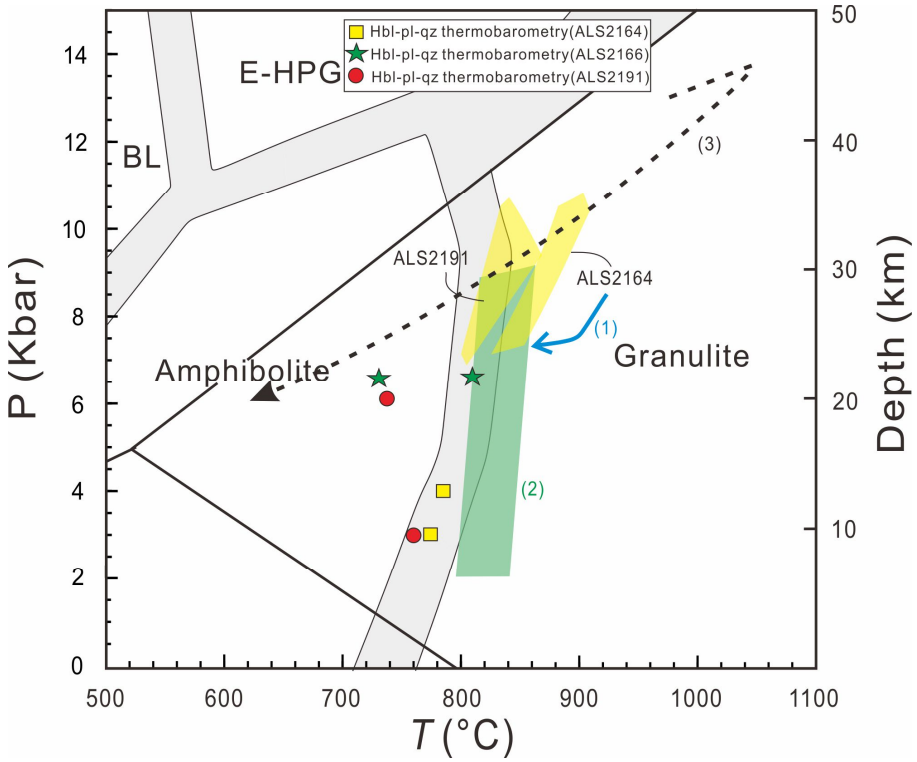

Figure 12. Summary of previously published metamorphic *P–T* paths and conditions (1–3), and metamorphic *PT* condition for amphibolites in the Diebusige (sample ALS2164) and Bayanwulashan (sample ALS2191) Complexes of the Alxa Block, NCC in this study: (1) corundum-bearing garnet–sillimanite gneiss in the Diebusige Complex [25]; (2) garnet-bearing magnetite quartzite in the Diebusige Complex [24]; (3) garnet-bearing mafic granulites in the Diebusige Complex [35]. Bl, blueschist facies; E–HPG, eclogite–high-pressure granulite-facies.

The NCC display two characteristics, including ca. 2.70–2.50 Ga magmatic-metamorphic events and ca. 1.95–1.85 Ga metamorphic events [22,79]. Although the Neoarchean TTG gneiss in the Alxa Block [27,30,31] is similar to those of the Yinshan Block, Dan et al. (2012) [36] considered that the Alxa Block was not the western extension of the Yinshan Block due to the absence of the Neoarchean greenstone belt and supracrustal rocks in the Alxa Block. Therefore, the extant data does not support the Alxa Block as the western extension of the Yinshan Block. The KB, a Paleoproterozoic orogenic belt in the Western Block of the NCC, mainly consists of the khondalite series (a set of upper amphibolite- to granulite-facies metasedimentary rocks, mafic granulite, charnockite, S-type granite, and a small amount of TTG gneiss) [22,79]. By comparing metamorphic age characteristics of the Alxa Block and the Western Block (Yinshan Block, KB, and Ordos Block) of the NCC (Figure 1a), Zou et al. (2021) [33] pointed out the metamorphic age characteristics of the Alxa Block is consistent with those in the KB, indicating

that they may have a similar metamorphic evolutionary history, at least in the Neoarchean–late Paleoproterozoic. Recently, several studies have reported HT–UHT metamorphic rocks with metamorphic ages of ca. 1.96–1.83 Ga (garnet-bearing magnetite quartzite, garnet-sillimanite-biotite-plagioclase gneiss, corundum-bearing gneiss and garnet-bearing mafic granulite) in the Diebusige Complex of the eastern Alxa Block [33–35], which is similar to the khondalite series of the KB.

The tectonic evolution of the KB includes the following processes: (1) the crustal thickening led to the burial of the protolith of khondalite series to the depth of the lower crust during syn-collision stage (ca. 1.96–1.95 Ga), which is characterized by formation of HP pelitic granulites [79,80]; (2) the underplating or emplacement of mantle-derived magmas resulted in the formation of UHT metamorphic rocks during the post-collisional extension stage (ca. 1.93–1.85 Ga) [81–83]. In this study, amphibolites have metamorphic ages of ca. 1.90–1.82 Ga, which are similar to previously reported metamorphic ages of ca. 1.96–1.83 Ga for HT–UHT rocks in the Diebusige Complex [32–34]. This indicates that the eastern Alxa Block likely experienced a shared HT–UHT metamorphism during the late Paleoproterozoic. Amphibolites in the Diebusige Complex display higher peak temperature but similar peak pressure, compared with those of amphibolites in the Bayanwulashan Complex, which indicates there is an extra heat source in the Diebusige Complex. However, both amphibolites from the two complexes recorded a higher geothermal gradient (~30 °C/km) than Phanerozoic continental crust (~20 °C/km) [84,85]. This high geothermal gradient is also supported by reported UHT metamorphic rocks and associated mantle-derived mafic-ultramafic rocks in the Diebusige Complex [33,34]. Additionally, the numerical modeling of Sizava et al. (2014) [85] showed that these high apparent thermal gradients can be achieved during the Paleoproterozoic hot orogensis. The HREE enrichment patterns of metamorphic zircons from the amphibolites in this study are in agreement with that these amphibolites formed under *PT* conditions where garnet is not stable (Figure 11) and at relatively shallower crust than those of the garnet-bearing mafic granulites in the Diebusige Complex [35]. Combining clockwise *P–T* paths of UHT metamorphic rocks in the Diebusige Complex (Figure 12) and metamorphic ages, an extensional setting after continental collision is inferred for these amphibolites in the eastern Alxa Block [84–86].

As discussion above, the Alxa Block is similar to the KB in that both have similar metamorphic rock types and experienced the late Paleoproterozoic tectonic thermal events. As several researchers have proposed, the late Paleoproterozoic metamorphic data from the Diebusige Complex [33–35] and this study suggest that the Alxa Block may be the westward extension of the KB [27,30,32–35]. Based on current speculation, there are still some issues which require clarification in future work, such as the occurrence of multiple magmatic-metamorphic events since the Neoproterozoic in the Alxa Block, has been served as an indicator that distinguishes the NCC [20,21,24–26].

8. Conclusions

(1) LA-ICP-MS zircon U–Pb dating yielded the metamorphic ages of ca. 1901–1817 Ma for amphibolites in the Diebusige and Bayanwulashan Complexes, representing the timing of amphibolite-facies metamorphism.

(2) Phase equilibrium modelling and conventional thermobarometries yielded a relatively large *PT* range for amphibolites in the Diebusige and Bayanwulashan Complexes, with a high geothermal gradient, which may correspond to an extensional setting following continental collision.

(3) The HREE enrichment patterns of metamorphic zircons are consistent with that these amphibolites formed under *PT* conditions where garnet is not stable and at relatively shallower crust than the garnet-bearing mafic granulites in the Diebusige Complex.

Supplementary Materials: The following supporting information can be downloaded at: https://www.mdpi.com/article/10.3390/min13111426/s1, Table S1: Major chemical compositions of clinopyroxene, hornblende, plagioclase and K-feldspar in the amphibolite sample ALS2164. Table S2: Major chemical compositions of clinopyroxene, hornblende, plagioclase and K-feldspar in the amphibolite sample ALS2166. Table S3: Major chemical compositions of hornblende, plagioclase and K-feldspar in the amphibolite sample ALS2191. Table S4: LA-ICP-MS zircon U–Pb isotope data of amphibolite samples ALS2164, ALS2166 and ALS2191. Table S5: LA-ICP-MS zircon trace element data of amphibolite samples ALS2164, ALS2166 and ALS2191. Table S6: Summary of Paleoproterozoic magmatic and metamorphic ages in the Alxa Block. References [27–30,33,35–37,39,42–51,53] are cited in the supplementary materials.

Author Contributions: Conceptualization, L.G.; Investigation, X.X. and Z.T.; Writing—original draft, F.Z. All authors have read and agreed to the published version of the manuscript.

Funding: This work was jointly supported by the National Natural Science Foundation of China (Grants No. 41772051 and 41890831) and a research grant from the State Key Laboratory of Continental Dynamics (SKLCD-04).

Data Availability Statement: Data is contained within the article or Supplementary Material. The data presented in this study are available in [Tables 1 and S1–S6].

Acknowledgments: The authors thank the editor and managing editor very much for their editorial work, and three anonymous reviewers for their constructive and insightful comments and suggestions.

Conflicts of Interest: The authors declare that the research was conducted in the absence of any commercial or financial relationships that could be construed as a potential conflict of interest.

References

1. Barker, A.J. *Introduction to Metamorphic Textures and Microstructures*; Blackie: Glasgow, UK, 1990.
2. Stowell, H.H.; Stein, E. The significance of plagioclase-dominant coronas on garnet, Wenatchee Block, northern Cascades, Washington, U. *S.A. Can. Mineral.* **2005**, *43*, 367–385. [CrossRef]
3. Kohn, M.J.; Spear, F. Two new barometers for garnet amphibolites with applications to eastern Vermont. *Am. Mineral.* **1990**, *75*, 89–96.
4. Surour, A.A. Medium- to high-pressure garnet-amphibolites from Gebel Zabara and Wadi Sikait, South Eastern Desert, Egypt. *J. Afr. Earth Sci.* **1995**, *21*, 443–457. [CrossRef]
5. Liu, J.; Bohlen, S.R.; Ernst, W.G. Stability of hydrous phases in subducting oceanic crust. *Earth Planet. Sci. Lett.* **1996**, *143*, 161–171. [CrossRef]
6. Dale, J.; Holland, T.; Powell, R. Hornblende–garnet–plagioclase thermobarometry: A natural assemblage calibration of the thermodynamics of hornblende. *Contrib. Mineral. Petrol.* **2000**, *140*, 353–362. [CrossRef]
7. Lopez, S.V.; Gomez, P.M.Y.; Azor, A.; Fernandez, S.J.M. Phase diagram sections applied to amphibolites: A case study from the Ossa_morena/Central Iberian Variscan suture (Southwestern Iberian Massif). *Lithos* **2003**, *68*, 1–21.
8. Winter, J.D. *An Introduction to Igneous and Metamorphic Petrology*, 2nd ed.; Prentice Hall: Upper Saddle River, NJ, USA, 2010; pp. 1–702.
9. Brown, M. The contribution of metamorphic petrology to understanding lithosphere evolution and geodynamics. *Geosci. Front.* **2014**, *5*, 553–569. [CrossRef]
10. Wei, C.J.; Guan, X.; Dong, J. HT-UHT metamorphism of metabasites and the petrogenesis of TTGs. *Acta Petrol. Sin.* **2017**, *33*, 1381–1404.
11. Zhang, B.T.; Ling, H.; Chen, P.; Hu, G.; Jiang, Y.; Yu, J. New recognition criteria for ortho and paraamphibolites: The Comparative study on mineral petrochemical characteristics of the precambrian orthoparaamphibolites from Xiangshan, Central Jiangxi Province. *Contrib. Geol. Miner. Resour. Res.* **2005**, *20*, 223–232.
12. Zhao, G.C.; Cawood, P.A.; Lu, L.Z. Petrology and P-T history of the Wutai amphibolites: Implications for tectonic evolution of the Wutai complex, China. *Precambrian Res.* **1999**, *93*, 181–199. [CrossRef]
13. Miyashiro, A. *Metamorphic Petrology*; UCL Press Limited: London, UK, 1994.
14. Qian, J.H.; Wei, C.J. P–t–t evolution of garnet amphibolites in the wutai–hengshan area, north china craton: Insights from phase equilibria and geochronology. *J. Metamorph. Geol.* **2016**, *34*, 423–446. [CrossRef]
15. Bader, T.; Zhang, L.F.; Li, X.W. Is the Songshugou Complex, Qinling Belt, China, an Eclogite Facies Neoproterozoic Ophiolite? *J. Earth Sci.* **2019**, *30*, 460–475. [CrossRef]
16. Lou, Y.; Wei, C.; Liu, X.; Zhang, C.; Tian, Z.; Wang, W. Metamorphic evolution of garnet amphibolite in the western Dabieshan eclogite belt, Central China: Evidence from petrography and phase equilibria modeling. *J. Asian Earth Sci.* **2013**, *63*, 130–138. [CrossRef]
17. Wang, Y.W.; Liu, L.; Liao, X.Y.; Gai, Y.S.; Yang, W.Q.; Kang, L. Multi-metamorphism of amphibolite in the Qinling complex,Qingyouhe area: Revelation from trace elements and mineral inclusions in zircons. *Acta Petrol. Sin.* **2016**, *32*, 1467–1492.

18. Wu, K.K.; Zhao, G.; Sun, M.; Yin, C.; He, Y.; Tam, P.Y. Metamorphism of the northern Liaoning Complex: Implications for the tectonic evolution of Neoarchean basement of the Eastern Block, North China Craton. *Geosci. Front.* **2013**, *4*, 305–320. [CrossRef]
19. Zhang, J.; Wei, C.J.; Chu, H. High-T and low-P metamorphism in the xilingol complex of central inner mongolia, China: An indicator of extension in a previous orogeny. *J. Metamorph. Geol.* **2018**, *36*, 393–417. [CrossRef]
20. Ge, X.H.; Liu, J.L. Broken "Western China Craton". *Acta Petrol. Sin.* **2000**, *16*, 59–66. (In Chinese with English Abstract)
21. Li, X.H.; Su, L.; Song, B.; Liu, D.Y. SHRIMP U-Pb zircon age of the Jinchuan ultramafic intrusion and its geological significance. *Chin. Sci. Bull.* **2004**, *49*, 420–422. [CrossRef]
22. Zhao, G.C.; Sun, M.; Wilde, S.A.; Li, S.Z. Late Archean to Paleoproterozoic evolution of the North China Craton: Key issues revisited. *Precambrian Res.* **2005**, *136*, 177–202. [CrossRef]
23. Zhao, G.C. Metamorphic evolution of major tectonic units in the basement of the north China craton: Key issues and discussion. *Acta Petrol. Sin.* **2009**, *25*, 1772–1792.
24. Dan, W.; Li, X.H.; Wang, Q.; Wang, X.C.; Wyman, D.A.; Liu, Y. Phanerozoic amalgamation of the Alxa block and North China Craton: Evidence from Paleozoic granitoids, U-Pb geochronology and Sr-Nd-Pb-Hf-O isotope geochemistry. *Gondwana Res.* **2016**, *32*, 105–121. [CrossRef]
25. Yuan, W.; Yang, Z.Y. The Alashan terrane was not part of north China by the late Devonian: Evidence from detrital zircon U-Pb geochronology and Hf isotopes. *Gondwana Res.* **2015**, *27*, 1270–1282. [CrossRef]
26. Liu, S.J.; Tsunogae, T.; Li, W.; Shimizu, H.; Santosh, M.; Wan, Y.S.; Li, J.H. Paleoproterozoic granulites from Heling'er: Implications for regional ultrahigh temperature metamorphism in the north China craton. *Lithos* **2012**, *148*, 54–70. [CrossRef]
27. Zhang, J.X.; Gong, J.H.; Yu, S.; Li, H.; Hou, K. Neoarchean–Paleoproterozoic multiple tectonothermal events in the western Alxa block, North China Craton and their geological implication: Evidence from zircon U–Pb ages and Hf isotopic composition. *Precambrian Res.* **2013**, *235*, 36–57. [CrossRef]
28. Dong, C.; Liu, D.Y.; Li, J.J.; Wang, Y.S.; Zhou, H.Y.; Li, C.D.; Yang, Y.H.; Xie, L.W. Palaeoproterozoic Khondalite Belt in the western North China Craton: New evidence from SHRIMP dating and Hf isotope composition of zircons from metamorphic rocks in the Bayan Ul-Helan Mountains area. *Chin. Sci. Bull.* **2007**, *52*, 2984–2994. (In Chinese with English Abstract) [CrossRef]
29. Geng, Y.S.; Wang, X.S.; Wu, C.M.; Zhou, X.W. Late-Paleoproterozoic tectonothermal events of the metamorphic basement in Alxa area: Evidence from geochronology. *Acta Petrol. Sin.* **2010**, *26*, 1159–1170. (In Chinese with English Abstract)
30. Zhang, J.X.; Gong, J.H. Revisiting the nature and affinity of the Alxa Block. *Acta Petrol. Sin.* **2018**, *34*, 940–962. (In Chinese with English Abstract)
31. Gong, J.H.; Zhang, J.X.; Yu, S.Y. The origin of Longshoushan Group and associated rocks in the southern part of the Alxa block: Constraint from LA-ICP-MS U-Pb zircon dating. *Acta Petrol. Mineral.* **2011**, *30*, 795–818. (In Chinese with English Abstract)
32. Zou, L.; Liu, P.H.; Liu, L.S.; Wang, W.; Tian, Z.H. Diagenetic and Metamorphic Timing of the Diebusige Complex, the Eastern Alxa Block: New Evidence from Zircon LA-ICP-MS U-Pb Dating of Biotite-Plagioclase Gneiss. *Earth Sci.* **2020**, *45*, 3313–3329. (In Chinese with English Abstract)
33. Zou, L.; Guo, J.H.; Liu, L.S.; Ji, L.; Liu, P.H. Palaeoproterozoic granulite-facies metamorphism in the eastern Alxa block: New petrological and geochronological evidence from the diebusige complex. *Precambrian Res.* **2021**, *354*, 106051. [CrossRef]
34. Zou, L.; Guo, J.H.; Jiao, S.J.; Huang, G.Y.; Tian, Z.H.; Liu, P.H. Paleoproterozoic ultrahigh-temperature metamorphism in the Alxa Block, the Khondalite Belt, North China Craton: Petrology and phase equilibria of quartz-absent corundum-bearing pelitic granulites. *J. Metamorph. Geol.* **2022**, *40*, 1159–1187. [CrossRef]
35. Wang, Y.; Ge, R.; Si, Y. Late Paleoproterozoic ultrahigh-temperature mafic granulite from the eastern Alxa Block, North China Craton. *Precambrian Res.* **2023**, *397*, 107172. [CrossRef]
36. Dan, W.; Li, X.H.; Guo, J.; Liu, Y.; Wang, X.C. Paleoproterozoic evolution of the eastern Alxa Block, westernmost North China: Evidence from in situ zircon U–Pb dating and Hf–O isotopes. *Gondwana Res.* **2012**, *21*, 838–864. [CrossRef]
37. Wu, S.; Hu, J.; Ren, M.; Gong, W.; Liu, Y.; Yan, J. Petrography and zircon U–Pb isotopic study of the Bayanwulashan Complex: Constrains on the Paleoproterozoic evolution of the Alxa Block, westernmost North China Craton. *J. Asian Earth Sci.* **2014**, *94*, 226–239. [CrossRef]
38. BGMRIM (Bureau of Geology and Mineral Resources of Inner Mongolia Autonomous Region). *Regional Geology of Inner Mongol Autonomous Region*; Geological Publishing House: Beijing, China, 1991. (In Chinese)
39. Gong, J.H.; Zhang, J.X.; Yu, S.Y.; Li, H.K.; Hou, K.J. Ca. 2.5 Ga TTG rocks in the western Alxa Block and their implications. *Chin. Sci. Bull.* **2012**, *57*, 4064–4076. (In Chinese with English Abstract) [CrossRef]
40. Gong, J.H.; Zhang, J.X.; Yu, S.Y. Redefinition of the" Longshoushan Group" outcropped in the eastern segment of Longshoushan on the southern margin of Alxa block: Evidence from detrital zircon U-Pb dating results. *Acta Petrol. Mineral.* **2013**, *32*, 1–22. (In Chinese with English Abstract)
41. Geng, Y.S.; Wang, X.S.; Shen, Q.H.; Wu, C.M. Redefinition of the Alxa Group-complex (Precambrian metamorphic basement) in the Alxa area, Inner Mongolia. *Geol. China* **2006**, *33*, 138–145.
42. Geng, Y.S.; Wan, X.S.; Shen, Q.H.; Wu, C.M. Chronology of the Precambrian metamorphic series in the Alxa area, Inner Mongolia. *Geol. China* **2007**, *34*, 251–261. (In Chinese with English Abstract)
43. Xiu, Q.; Yu, H.; Li, Q.; Zuo, G.; Li, J.; Cao, C. Discussion on the petrogenic time of Longshoushan Group, Gansu Province. *Acta Geol. Sin.* **2004**, *78*, 366–373. (In Chinese with English Abstract)

44. Liu, Y. Characteristics and Their Geological Significance of Paleoproterozoic Granite in Jinchuan, Gansu Province. Master's Thesis, University of Geosciences, Beijing, China, 2008. (In Chinese with English Summary)
45. Gong, J.; Zhang, J.; Wang, Z.; Yu, S.; Li, H.; Li, Y. Origin of the Alxa Block, western China: New evidence from zircon U–Pb geochronology and Hf isotopes of the Longshoushan Complex. *Gondwana Res.* **2016**, *36*, 359–375. [CrossRef]
46. Liu, J.; Yin, C.; Zhang, J.; Qian, J.; Li, S.; Xu, K.; Wu, S.; Xia, Y. Tectonic evolution of the Alxa Block and its affinity: Evidence from the U-Pb geochronology and Lu-Hf isotopes of detrital zircons from the Longshoushan Belt. *Precambrian Res.* **2020**, *344*, 105733. [CrossRef]
47. Zeng, R.; Lai, J.; Mao, X.; Li, B.; Zhang, J.; Bayless, R.C.; Yang, L. Paleoproterozoic multiple Tectonothermal events in the Longshoushan Area, Western North China Craton and their geological implication: Evidence from geochemistry, Zircon U–Pb geochronology and Hf Isotopes. *Minerals* **2018**, *8*, 361. [CrossRef]
48. Shen, Q.H.; Geng, Y.S.; Wang, X.S.; Wu, C.M. Petrology, geochemistry, formation environment and ages of Precambrian amphibolites in Alxa region. *Acta Petrol. Mineral.* **2005**, *24*, 21–31. (In Chinese with English Abstract)
49. Zhou, H.Y.; Mo, X.X.; Li, J.J.; Li, H.M. The U-Pb isotopic dating age of single zircon from biotite plagioclase gneiss in the Qinggele area, Alashan, western Inner Mongolia. *Bull. Mineral. Petrol. Geochem.* **2007**, *26*, 221–223. (In Chinese with English Abstract)
50. Li, J.J.; Shen, B.F.; Li, H.M.; Zhou, H.Y.; Guo, L.J.; Li, C.Y. Single-zircon U–Pb age of granodioritic gneiss in the Bayan Ul area, western Inner Mongolia. *Geol. Bull. China* **2004**, *23*, 1243–1245. (In Chinese with English Abstract)
51. Bao, C.; Chen, Y.L.; Li, D.P. LA-MC-ICP-MS zircons U-Pb dating and Hf isotopic compositions of the Paleoproterozoic amphibolite in Bayan Ul area, Inner Mongolia. *Geol. Bull. China* **2013**, *32*, 1513–1524.
52. Liu, Y.S.; Gao, S.; Hu, Z.C.; Gao, C.G.; Zong, K.Q.; Wang, D.B. Continental and oceanic crust recycling-induced melt-peridotite interactions in the Trans-North China Orogen: U-Pb dating, Hf isotopes and trace elements in zircons of mantle xenoliths. *J. Petrol.* **2010**, *51*, 537–571. [CrossRef]
53. Whitney, D.L.; Evans, B.W. Abbreviations for names of rock-forming minerals. *Am. Mineral.* **2010**, *95*, 185–187. [CrossRef]
54. Leake, B.E.; Woolley, A.R.; Arps CE, S.; Birch, W.D.; Gilbert, M.C.; Grice, J.D.; Guo, Y.Z. Nomenclature of amphiboles: Report of the subcommittee on amphiboles of the International Mineralogical Association, Commission on New Minerals and Mineral Names. *Can. Mineral.* **1997**, *35*, 219–246.
55. Anderson, E.D.; Moecher, D.P. Omphacite breakdown reactions and relation to eclogite exhumation rates. *Contrib. Mineral. Petrol.* **2007**, *154*, 253–277. [CrossRef]
56. Gayk, T.; Kleinschrodt, R.; Langosch, A.; Seidel, E. Quartz exsolution in clinopyroxene of high-pressure granulite from the Munchberg Massif. *Eur. J. Mineral.* **1995**, *7*, 1217–1220. [CrossRef]
57. Nakano, N.; Osanai, Y.; Owada, M. Multiple breakdown and chemical equilibrium of silicic clinopyroxene under extreme metamorphic conditions in the Kontum Massif, central Vietnam. *Am. Mineral.* **2007**, *92*, 1844–1855. [CrossRef]
58. Page, F.Z.; Essene, E.J.; Mukasa, S.B. Prograde and retrograde history of eclogites from the Eastern Blue Ridge, North Carolina, USA. *J. Metamorph. Geol.* **2003**, *21*, 685–698. [CrossRef]
59. Page, F.Z.; Essene, E.J.; Mukasa, S.B. Quartz exsolution in clinopyroxene is not proof of ultrahigh pressures: Evidence from eclogites from the Eastern Blue Ridge, Southern Appalachians, USA. *Am. Mineral.* **2005**, *90*, 1092–1099. [CrossRef]
60. Proyer, A.; Krenn, K.; Hoinkes, G. Orientated precipitates of quartz and amphibole in clinopyroxene of metabasites from the Greek Rhodope: A product of open system precipitation during eclogite-granulite-amphibolite transition. *J. Metamorph. Geol.* **2009**, *27*, 639–654. [CrossRef]
61. Faryad, S.W.; Fisera, M. Olivine-bearing symplectites in fractured garnet from eclogite Moldanubian zone (Bohemian massif)—A short-lived, granulite facies event. *J. Metamorph. Geol.* **2015**, *33*, 597–612. [CrossRef]
62. De Capitani, C.; Petrakakis, K. The computation of equilibrium assemblage diagrams with Theriak/Domino software. *Am. Mineral.* **2010**, *95*, 1006–1016. [CrossRef]
63. Holland, T.J.B.; Powell, R. An internally consistent thermodynamic data set for phases of petrological interest. *J. Metamorph. Geol.* **1998**, *16*, 309–343. [CrossRef]
64. Holland, T.J.B.; Powell, R. An improved and extended internally consistent thermodynamic dataset for phases of petrological interest, involving a new equation of state for solids. *J. Metamorph. Geol.* **2011**, *29*, 333–383. [CrossRef]
65. Green, E.C.R.; White, R.W.; Diener, J.F.A.; Powell, R.; Holland, T.J.B.; Palin, R.M. Activity–composition relations for the calculation of partial melting equilibria in metabasic rocks. *J. Metamorph. Geol.* **2016**, *34*, 845–869. [CrossRef]
66. White, R.W.; Powell, R.; Holland, T.J.B.; Johnson, T.E.; Green, E.C.R. New mineral activity–composition relations for thermodynamic calculations in metapelitic systems. *J. Metamorph. Geol.* **2014**, *32*, 261–286. [CrossRef]
67. Holland, T.J.B.; Powell, R. Activity–composition relations for phases in petrological calculations: An asymmetric multicomponent formulation. *Contrib. Mineral. Petrol.* **2003**, *145*, 492–501. [CrossRef]
68. White, R.W.; Powell, R.; Clarke, G.L. The interpretation of reaction textures in Fe-rich metapelitic granulites of the Musgrave Block, central Australia: Constraints from mineral equilibria calculations in the system K_2O–FeO–MgO–Al_2O_3–SiO_2–H_2O–TiO_2–Fe_2O_3. *J. Metamorph. Geol.* **2002**, *20*, 41–55. [CrossRef]
69. White, R.W.; Powell, R.; Holland TJ, B.; Worley, B.A. The effect of TiO_2 and Fe_2O_3 on metapelitic assemblages at greenschist and amphibolite facies conditions: Mineral equilibria calculations in the system K_2O–FeO–MgO–Al_2O_3–SiO_2–H_2O–TiO_2–Fe_2O_3. *J. Metamorph. Geol.* **2000**, *18*, 497–511. [CrossRef]

70. Korhonen, F.J.; Brown, M.; Clark, C.; Bhattacharya, S. Osumilite–melt interactions in ultrahigh temperature granulites: Phase equilibria modelling and implications for the P–T–t evolution of the Eastern Ghats Province, India. *J. Metamorph. Geol.* **2013**, *31*, 881–907. [CrossRef]
71. Holland, T.J.B.; Blundy, J.D. Non-ideal interactions in calcic amphiboles and their bearing on amphibole-plagioclase thermometry. *Contrib. Mineral. Petrol.* **1994**, *116*, 433–447.
72. Bhadra, S.; Bhattacharya, A. The barometer tremolite + tschermakite + 2 albite = 2 pargasite + 8 quartz: Constraints from experimental data at unit silica activity, with application to garnet-free natural assemblages. *Am. Mineral.* **2007**, *92*, 491–502. [CrossRef]
73. Liao, Y.; Wei, C.J.; Rehman, H.U. Titanium in calcium amphibole: Behavior and thermometry. *Am. Mineral.* **2021**, *106*, 180–191.
74. Ferry, J.M.; Watson, E.B. New thermodynamic models and revised calibrations for the Ti-in-zircon and Zr-in-rutile thermometers. *Contrib. Mineral. Petrol.* **2007**, *154*, 429–443. [CrossRef]
75. Gao, X.Y.; Zheng, Y.F. On the Zr-in-rutile and Ti-in-zircon geothermometers. *Acta Petrol. Sin.* **2011**, *27*, 417–432. (In Chinese with English Abstract)
76. Sun, S.S.; McDonough, W.F. Chemical and isotopic systematics of oceanic basalts: Implications for mantle composition and processes. *Geol. Soc. Lond. Spec. Publ.* **1989**, *42*, 313–345. [CrossRef]
77. Guevara, V.E.; Caddick, M.J. Shooting at a moving target: Phase equilibria modelling of high-temperature metamorphism. *J. Metamorph. Geol.* **2016**, *34*, 209–235.
78. Palin, R.M.; Weller, O.M.; Waters, D.J.; Dyck, B. Quantifying geological uncertainty in metamorphic phase equilibria modelling: A Monte Carlo assessment and implications for tectonic interpretations. *Geosci. Front.* **2016**, *7*, 591–607.
79. Zhao, G.C.; Cawood, P.A.; Li, S.Z.; Wilde, S.A.; Sun, M.; Zhang, J.; He, Y.H.; Yin, C.Y. Amalgamation of the North China Craton: Key issues and discussion. *Precambrian Res.* **2012**, *222–223*, 56–76.
80. Yin, C.Q.; Zhao, G.C.; Wei, C.J.; Sun, M.; Guo, J.H.; Zhou, X.W. Metamorphism and partial melting of high-pressure pelitic granulites from the Qianlishan Complex: Constraints on the tectonic evolution of the Khondalite Belt in the North China Craton. *Precambrian Res.* **2014**, *242*, 172–186.
81. Santosh, M.; Wilde, S.; Li, J. Timing of Paleoproterozoic ultrahigh-temperature metamorphism in the North China Craton: Evidence from SHRIMP U-Pb zircon geochronology. *Precambr. Res.* **2007**, *159*, 178–196. [CrossRef]
82. Gou, L.L.; Zi, J.W.; Dong, Y.P.; Liu, X.M.; Li, Z.H.; Xu, X.F.; Zhang, C.L.; Liu, L.; Long, X.P.; Zhao, Y.H. Timing of two separate granulite-facies metamorphic events in the Helanshan complex, North China Craton: Constraints from monazite and zircon U-Pb dating of pelitic granulites. *Lithos* **2019**, *350–351*, 105216.
83. Jiao, S.J.; Fitzsimons, I.C.W.; Guo, J.H. Paleoproterozoic UHT metamorphism in the Daqingshan Terrane, North China Craton: New constraints from phase equilibria modeling and SIMS U-Pb zircon dating. *Precambrian Res.* **2017**, *303*, 208–227.
84. Zheng, Y.F.; Zhao, G.C. Two styles of plate tectonics in Earth's history. *Sci. Bull.* **2020**, *65*, 329–334. [CrossRef]
85. Sizova, E.; Gerya, T.; Brown, M. Contrasting styles of Phanerozoic and Precambrian continental collision. *Gondwana Res.* **2014**, *25*, 522–545.
86. Thompson, A.B.; England, P.C. Pressure–temperature–time paths of regional metamorphism II. *Their inference and interpretation using mineral assemblages in metamorphic rocks. J. Petrol.* **1984**, *25*, 929–955.